

Cardiac Muscle Cell-Based Coupled Oscillator Network for Collective Computing

Xiang Ren, Jorge Gomez, Mohammad Khairul Bashar, Jiaying Ji, Uryan Isik Can, Hsueh-Chia Chang, Nikhil Shukla, Suman Datta, and Pinar Zorlutuna*

Current rate of data generation and the need for real-time data analytics can benefit from new computational approaches where computation proceeds in a massively parallel way while being scalable and energy efficient. Biological systems arising from interaction of living cells can provide such pathways for sustainable computing. Current designs for biocomputing leveraging the information processing units of the cells, such as DNA, gene, or protein circuitries, are inherently slow (hours to days speed) and, therefore, are primarily being considered for archival storage of information. On the contrary, electrically active cells that can synchronize in milliseconds and can be connected as networks to perform massively parallel tasks can transform biocomputing and lead to novel ways of high throughput information processing. Herein, coupled oscillator networks made of living cardiac muscle cells, or bio-oscillators, is explored as collective computing components for solving computationally hard problems. An empirically validated circuit compatible macromodel is developed for the bio-oscillators and the fibroblast cells acting as coupling elements, to faithfully reproduce the synchronization dynamics of the network and it is shown that such bio-oscillator network can be scaled up to hundreds of nodes and be used to solve computationally hard problems faster than traditional heuristics-based Boolean algorithms.

Conventional complementary metal oxide semiconductor (CMOS) transistors working in the Boolean paradigm and guided by Moore's law constitute the backbone of our current computational framework. However, certain classes of computational problems are fundamentally difficult to solve in the Boolean framework. Constrained optimization problems like vertex coloring of graphs, which is the task of assigning colors to the vertices of the graph such that no two vertices sharing the same

edge have the same color, belong to the class of combinatorial optimization problems.^[1] Such compute tasks find extensive applications in many real-world problems such as fault diagnosis, scheduling, and resource allocation. However, these problems fundamentally exhibit NP-hard (non-deterministic polynomial time) complexity. This implies that even the best algorithms end up searching the vast solution space in a greedy fashion for certain problem instances. Consequently, this manifests itself as an exponential increase in solution-time and computational resource with increasing size of the problem, when solved in the conventional Boolean computing framework. In contrast to the inherently sequential approach of digital CMOS which takes incremental discrete steps following the algorithm as the computation proceeds, the computational properties of the coupled oscillators arise from their rich spatiotemporal dynamics that enables the system to search in a highly parallel fashion, the high-dimensional configuration space that characterizes combinatorial optimization problems, and the driven by the dynamics synchronization drives the continuous time trajectory to settle at or close to the global minima.

Biological systems have been inspiring many approaches that aim to build new computing modules using synthetic biology.^[2,3] Most of the research so far in this area aims to create data storage or basic logic units that are built by engineering the genetic elements of single cells, including bacteria and mammalian cells.^[4]

Dr. X. Ren, J. Ji, Dr. U. I. Can, Prof. H.-C. Chang, Prof. P. Zorlutuna
 Department of Aerospace and Mechanical Engineering
 University of Notre Dame
 Notre Dame, IN 46556, USA
 E-mail: pinar.zorlutuna.1@nd.edu

 The ORCID identification number(s) for the author(s) of this article can be found under <https://doi.org/10.1002/aisy.202000253>.

© 2021 The Authors. Advanced Intelligent Systems published by Wiley-VCH GmbH. This is an open access article under the terms of the Creative Commons Attribution License, which permits use, distribution and reproduction in any medium, provided the original work is properly cited.

DOI: [10.1002/aisy.202000253](https://doi.org/10.1002/aisy.202000253)

J. Gomez, Prof. S. Datta
 Department of Electrical Engineering
 University of Notre Dame
 Notre Dame, IN 46556, USA

M. K. Bashar, Prof. N. Shukla
 Department of Electrical and Computer Engineering
 University of Virginia
 Charlottesville, VA 22904, USA

Prof. H.-C. Chang, Prof. P. Zorlutuna
 Department of Chemical and Biomolecular Engineering
 University of Notre Dame
 Notre Dame, IN 46556, USA

For example, Fan et al. manipulated the nanostructure of single cells to achieve DNA/RNA logic operations.^[5] Willner et al. constructed DNA circuits to perform AND, NAND, NOR, and XOR gates for biocomputing, which theoretically can expand to full arithmetic logic units to perform digital logic operations.^[6] Fussenegger et al. constructed AND, OR, NOR gates, programmable full adder, and analog-to-digital converters using 3D cell culture.^[7] Can et al. used micropatterned heart cells to create a diode analog.^[8] Although through these studies biocomputing principles/systems have been established for studying the basic logic operations, the ability to solve hard problems using biocomputing is conspicuously missing. To address this, here we present a novel tissue-level biological computing system using living heart cells as oscillatory units for solving computationally hard problems.

Our research is inspired by the natural ability of physical systems including biological systems, to minimize their own energy—a process that finds a natural analog to problems such as optimization and learning.^[9] While such behavior has been observed in dynamical systems such as coupled oscillators and Hopfield Networks, this collective paradigm finds many natural analogs in biological systems such as decision-making mechanisms of neural networks,^[10] the swarm intelligence of bacterial colonies,^[11] synthetic genetic oscillators in single cells,^[12] decision-making unicellular amoeboid organism for demanding problems,^[13] and the rhythmic beating of the cardiac muscle (CM) cells,^[14] with the added advantage of ultralow energy requirements which are difficult to achieve in conventional solid-state devices and circuits. Therefore, in this work, we aimed to harness the synchronized beating of living heart cells as a natural ultralow energy (< nJ/bio-oscillator) biological hardware platform to implement continuous time dynamical system for solving computationally hard problems. The coupled relaxation oscillators exhibit a unique ordering of oscillator phases such that adjacent nodes (oscillators) belong to an independent set. In other words, the phase ordering (produced by the oscillators) is such that independent sets of the graph appear in a cyclic order. As explained in our prior work that explored such algorithms using vanadium dioxide (VO_2) oscillators,^[1,15] these dynamics arise from the equivalence between the eigenvalues of the adjacency matrix of the graph and the eigenvalues of the matrix describing the dynamics of the oscillators in state space.^[16] Consequently, this phase ordering can be partitioned into various independent sets and assigning a color to each set approximates the near-/optimal solution to the minimum vertex coloring problem.^[17] In this study, we explored the potential of heart muscle cells and their synchronization dynamics to map a computational problem to a biological system using living heart cells as the oscillatory units. The coupled network of the oscillating cardiac cells can be leveraged as a biological computational fabric wherein the intrinsic energy minimization tendencies of the system can be exploited for computing problems such as graph analytics that require a highly parallel computing hardware. In the biological coupled oscillator fabric, the oscillating cardiac cells can be mapped to the graph nodes, the ionic channels to the coupling among the oscillators, and the distinct relative phases among the beating of the cells would represent the coloring solution to the graph.

CM cells are electrically active components that can initiate and relay electrical signals without loss. More interestingly, they spontaneously beat (i.e., oscillate) at a stable pace, and when coupled with each other, they synchronize to a locked, steady frequency. On the contrary, cardiac fibroblast (CF) cells in the heart are support cells that fill in the space between the CMs and provide electrical pathways for ionic diffusion in between adjacent cells through the gap junctions that they make with the muscle cells. The CF cells are not oscillatory (i.e., not beating), but they passively couple the beating CM cells.^[8] In this study, we designed two kinds of computational elements, oscillators and coupling elements, to implement a coupled oscillator network. The beating CM cells function as oscillators, while the CF bridges in between function as coupling elements (Figure 1). The CF bridges between the CM clusters enable electrical conduction via ion exchange and provide a resistor–capacitor (RC)-type coupling between the oscillatory elements. The distance between the CM clusters or the length of the CF bridges modulates the strength of coupling between the clusters (Figure 2).

To create the coupled bio-oscillators, as a model cell source, we used neonatal rat ventricular cardiac cells that were isolated from 2-day-old Sprague-Dawley rat hearts following a previously established protocol^[18] in compliance with the Institutional Animal Care and Use Committee (IACUC) guidelines and under an approved protocol from the University of Notre Dame. The isolated cell mixture of rat CMs and rat CFs was preplated for 2 h in culture conditions to enrich the CMs in the cell mixture. At the end of 2 h preplating, the ratio of CM to CF was about 7:3. The CM-enriched cardiac cell mixture was collected from the culture flasks, and suspended in the culture medium of Dulbecco's Modified Eagle Medium (DMEM) with 10% fetal bovine serum (FBS) and 1% penicillin, and used as the cell source throughout the study.

To study the continuous time synchronization dynamics, we recorded the changes in the membrane potential of CMs, first as individual clusters and then as connected clusters through CF bridges, in real time. To create a well-defined network of connected cell clusters and monitor their spatial and temporally resolved dynamics of oscillation, we start by patterning the CMs and CFs on glass substrates with an embedded microelectrode array (MEA). To control the cell localization, we used polydimethylsiloxane (PDMS) blockers with varying width (150–400 μm) and fixed height (120 μm) to partially cover a cell adhesive protein micropattern (Figure 1). The PDMS blockers were fabricated with SU-8 3050 photoresist on silicon prime wafers using standard photolithography. The blockers were manually placed on the MEA substrate to block the parts of the substrate where we want to avoid the CM presence. Then, 10% fibronectin diluted in phosphate-buffered saline (PBS) was used to treat the unblocked parts of the MEA substrate in a 37 °C incubator for 30 min to enable CM attachment on the MEA substrate as separate clusters. The culture medium was refreshed after majority of the CMs, and CFs (7:3 mixture) were attached to the MEA substrate. The CMs within the CM–CF clusters start to beat after 1.5–2 days of culture. Then, the PDMS blocker was carefully removed by a sterile tweezer, without interfering with the beating cell clusters. Once the blocker is removed in between the cell clusters, CFs in the CM–CF mixture will proliferate and migrate

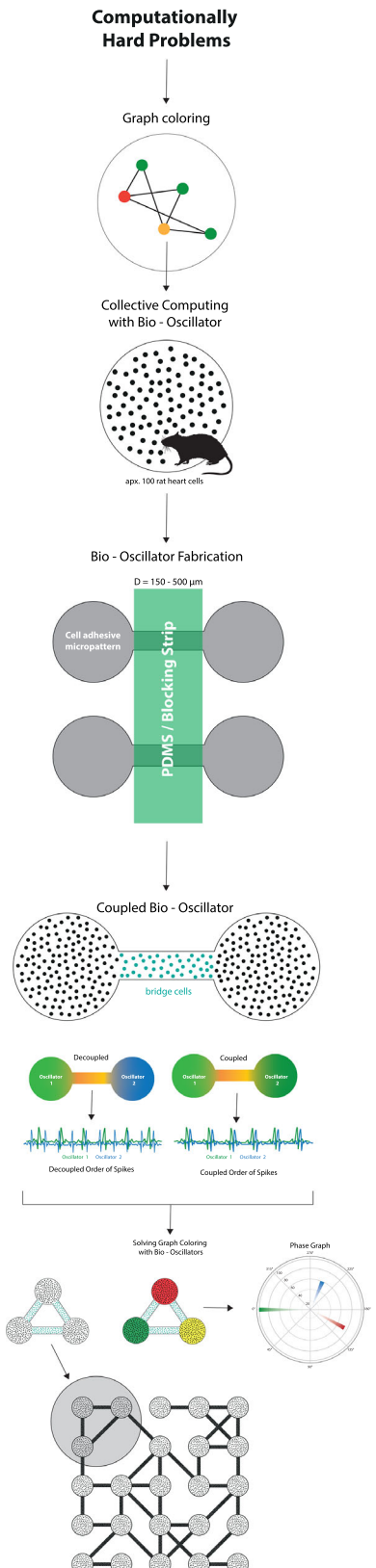


Figure 1. Illustration of the programmable biocomputing logic using pre-patterned rCM and rCF.

to fill in the gap, therefore bridging the beating cell clusters. The cell membrane potential was continuously measured by MEA-2100 system (Multichannel Systems) with a sampling rate of 1 kHz up to 72 h. This way, we were able to record the membrane potential changes in the beating CMs before and after their coupling through an RC element, namely, the CFs as the bridge cells, and analyzed this membrane potential data for frequency and phase lag information for two (Figure 2), three and four clusters (Figure 3) of bio-oscillators.

To study the impact of the coupling strength (i.e., length of the CF bridge) on the synchronization dynamics of beating clusters, we first analyze the case of pairwise coupled clusters (Figure 2). We consider four different scenarios defined by different fibroblast insert lengths: 150, 200, 300, and 400 μm . The first column of Figure 2a shows the topologies of cell patterns used for each case. The clusters are shown using colors red and blue, and the coupling is shown in yellow. To monitor the synchronization of the clusters we are interested in the action potential (AP) which is the potential difference across the membrane of the cell; however, the techniques that would allow us to measure it directly, such as patch clamp technique, would disturb the cells and adversely affect the synchronization dynamics.^[19] For that reason, we monitored the cell activity, by measuring the extracellular electric potential known as field potential (FP) using a commercial MEA that enables noninvasive and long-term measurements. From the measured FP, we can extract the period and phase of the AP^[20] which is the only read out that is needed for using this system for computing. The second column of Figure 2a shows the experimental FP for each one of these topologies. To extract the phase and period of oscillation for the bio-oscillators, we used two methods: Fourier transform and peak detection. The spectrogram for each electrode allows us to identify the regions in which the cells clusters are beating and synchronized, thereby enabling us to select the electrodes that will capture the representative cluster dynamics. The third column of Figure 2a shows an example of synchronization of the two clusters in frequency domain as obtained from fast Fourier transform (FFT). The fourth column of Figure 2a shows the evolution of the frequency of both clusters, in which the synchronized regions are shown in green. The clusters can synchronize at different frequencies in a range of 0.3–4.5 Hz. Finally, using peak detection over the normalized waveform in the selected electrodes, we extract the phase difference between the clusters for different frequencies (cf. pseudocode in supporting information).

We plot the synchronization frequencies for each fibroblast width in Figure 2b. Although there is a variation in the extracted phase–frequency points, we can conclude in a statistically significant fashion that: 1) the phase between the clusters is modulated by the fibroblast length; and 2) the phase between the clusters is also modulated by the frequency. We fit the phase–frequency relation to an exponential equation as given as follows

$$\text{Ph} = \alpha e^{\beta f} \quad (1)$$

where Ph is the phase, f is the frequency, and α and β are fitting parameters. The fitting parameters for each fibroblast length are shown in Table 1.

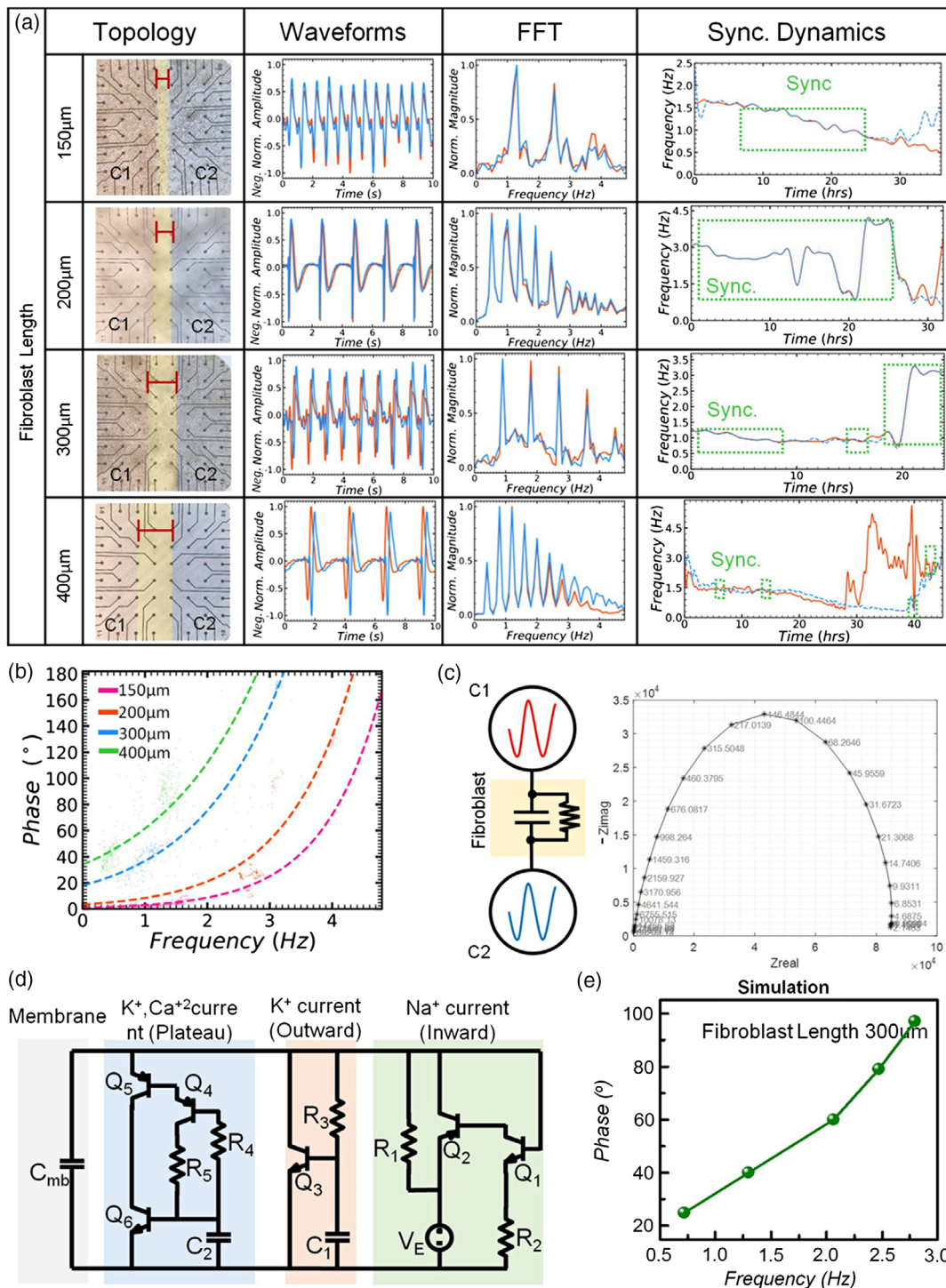


Figure 2. Computational Core: a) synchronization dynamics of two clusters of cells (C1 (red) and C2 (blue)) separated by fibroblast (yellow) of different lengths. The different columns show: i) experimental setup of the two clusters separated by fibroblast, ii) example of temporal waveforms for each one of the clusters, iii) Fourier transform of the waveforms showed in (ii), iv) evolution of frequency for each one of the clusters during the experiment; the cluster are considered synchronized when both frequencies are equal; examples of synchronized regions are shown in green. b) Phase dependence on frequency and fibroblast length for the configurations presented in (a). c) Extraction of fibroblast RC coupling parameters that will be used for the simulations. d) The simulation of phase dependence on frequencies with fibroblast length of 300 μ m for the two-cluster pattern. e) The equivalent circuit of a two-cluster pattern.

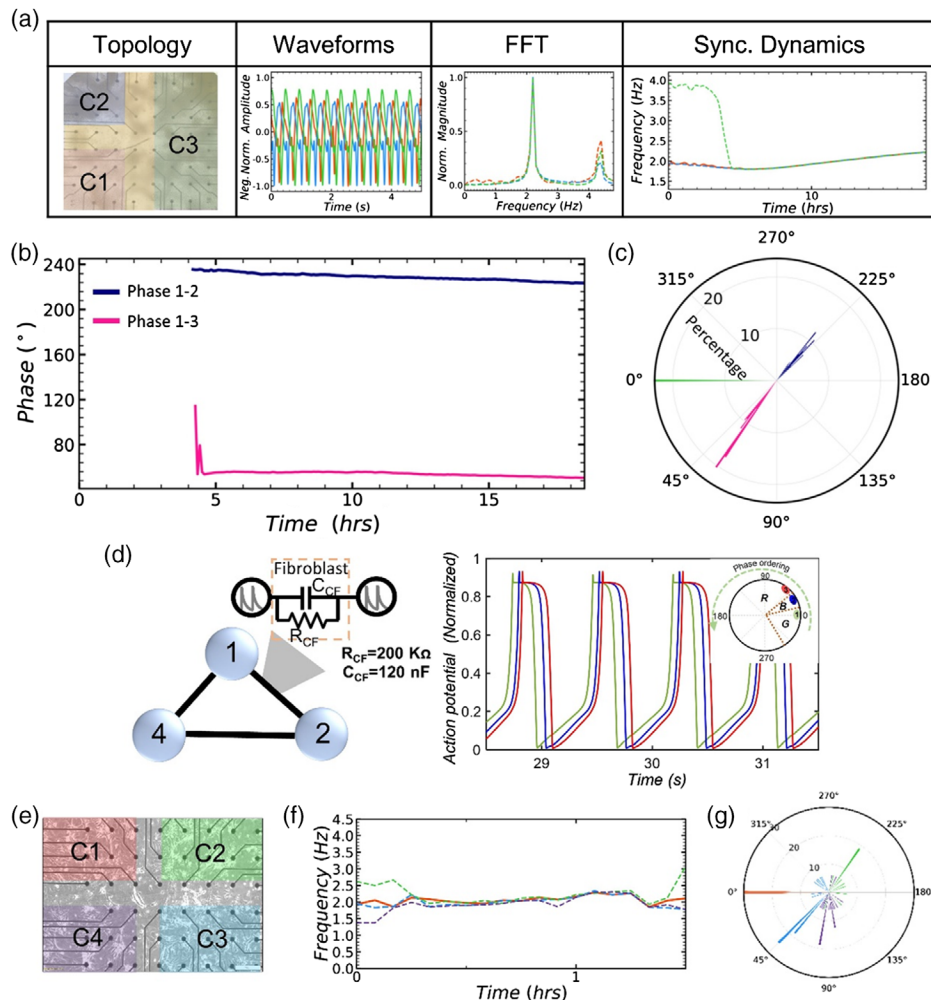


Figure 3. Three oscillators synchronization: a) synchronization dynamics of three clusters of cells (C1 (red), C2 (blue), and C3 (green)) separated by fibroblast (yellow). The different columns show: i) experimental setup of the three clusters separated by fibroblasts, ii) example of temporal waveforms, iii) Fourier transform of the waveforms showed in (ii), iv) evolution of frequency for each one of the clusters during the experiment. b) Evolution of phase over time. c) Polar plot of the phase differences shown in (b). d) The simulation results of a three-cluster oscillator and coloring solutions. e) Experimental setup of the four clusters separated by cardiac fibroblasts. f) Evolution of frequency for each cluster during the experiment; color coded with red, green, blue, and purple. g) Polar plot of the phase differences of the four-cluster network.

Table 1. Extracted parameters for data fitting Figure 2b.

Fibroblast length [μm]	α	β
150	1	1
200	3	0.9
300	18	0.7
400	34	0.6

We measure the impedance of the proliferated CF to model the electrical nature of coupling between the two oscillator clusters. As shown in Figure 2c, the Nyquist plot reveals that the CF presents itself as an RC filter between the two beating oscillatory clusters. The conductance per unit length and the ability to form gap junctions between the CF and CF, or between the CM and CF, determine the maximum limit of the CF insert length

between two clusters.^[21] Insert sizes longer than $400 \mu\text{m}$ in length resulted in unsynchronized clusters (data not shown).

To simulate the oscillations in the AP of the cardiac cell, we implement the equivalent circuit model of the cardiac cell proposed by Maeda et al.^[22] in SPICE. The circuit (Figure 2d) replicates using electronic components the three different currents arising from the sodium, potassium, and calcium currents across the membrane. Tuning resistor R_1 and C_1 (in Figure 2e) helps us modulate the oscillation frequency of the cell 0.3–3 Hz. Furthermore, the oscillators coupled using a fibroblast layer is modeled a parallel combination of a resistor and capacitor. The impedance of this combination is obtained using impedance spectroscopy (described in detail in the Supporting Information); the Cole–Cole plots in Figure 2c reveal $R_{CF} = 200 \text{ k}\Omega$ and $C_{CF} = 120 \text{ nF}$. Using the aforementioned simulation framework, we generate the phase–frequency characteristics for a pair of coupled oscillators coupled with $300 \mu\text{m}$ fibroblasts. It can be

observed that simulations in Figure 2e exhibit a good qualitative match to the experimental trends observed in Figure 2b.

Spontaneous and continuous AP generation (i.e., beating) of living cardiac cells makes them ideal candidates as biocomputational analog of oscillators. These bio-oscillators communicate through ion channels and synchronize to a steady frequency (i.e., couple). This communication is possible through gap junctions, intracellular pores, which allow ion diffusion. After formed, the CM clusters initiate beating frequencies independently. The CM cells are nondividing cells, which remain attached to the fibronectin-coated regions of the MEA substrate. The CF, on the contrary, proliferative cells occupy the regions previously covered by PDMS blockers. Once the CF cells proliferate and connect the two clusters together, the gap junctions between the CF and CM electrically couple the two and initiate ion exchange between the CM clusters. The CM beating frequency starts to shift and both clusters synchronize to another frequency. This new frequency is not necessarily the frequency of either initial beating frequency, which arises from the synchronization dynamics rather than a master-slave latch behavior.

Based on the two-cluster oscillator results, we selected 300 μm of fibroblast length to implement the three clusters network (Figure 3a–d) and the four clusters network (Figure 3e–g). The first column of Figure 3a demonstrates the topology of the three clusters we built on the MEA. The clusters, C1, C2, and C3, are presented in different colors (red, blue, and green), respectively. The second column in Figure 3b presents the waveform of the FP of each cluster. The third column is the Fourier transform of a specific temporal snapshot of the three clusters in which they are synchronized. The fourth column shows the frequency alterations of each cluster during the long-term FP monitoring. We used cluster C1 as the reference cluster to measure the phase differences. Figure 3b shows the phase evolutions of C2 and C3 compared with C1 over the entire experiment. The same data in a polar histogram is shown Figure 3c with a resolution of 1°. The height of the histogram represents the percentage of the synchronization time that the phases are at a specific angle. The dispersion of the phases is narrow over 18 h of the experiment. In this experiment, the dimensions of the clusters are asymmetric, which reflects on the synchronization phases. Figure 3e–g shows the construction of four-cluster network on MEA. Similar to the three-cluster network, we used cluster C1 (red) as the reference cluster to measure the phase differences of cluster C2 (green), C3 (blue), and C4 (purple) in the four-cluster network. The phase differences in Figure 3g indicate the four clusters are synchronized with a major difference of phase delay around 45°, 85°, and 230°.

Although in this study we used microelectrode-based FP recording to precisely study the coupling dynamics, the optimized system can use simple microscopy imaging to extract the phase and frequency information, such as calcium transient imaging (Figure S3, Supporting Information), for future applications where direct interface with traditional electronic devices is not needed. Using imaging as a read-out strategy could potentially increase the throughput as well as reduce the cost of device fabrication. On the contrary, ability to directly interphase with such traditional electronic devices might be an advantage and desired for applications where such read-outs would be valuable. In this study, we performed short-term calcium imaging (5 min

before and 5 min after the synchronization) studies on the coupled oscillators to show the functional integrity of the cells in our system and as a proof of concept for an alternative high throughput read-out strategy in future studies.

Furthermore, using the simulation framework described earlier, we simulate the synchronization dynamics of the fibroblast-coupled three oscillator system (Figure 3d). The simulation shows a good qualitative match to the experimental data revealing nonzero phase differences between each oscillator in the network. More importantly, the simulation and experiments show a phase ordering of the oscillators that can be leveraged for computing as illustrated in the following section.

Figure 4 simulates the application of the CF-coupled cardiac cell oscillators to solve the minimum vertex coloring problem in a graph. This problem entails computing the minimum number of colors required to be assigned to the edges such that no two adjacent vertices (i.e., vertices that share an edge) are assigned the same color. To solve this problem using the bio-oscillators, the graph is mapped on to the network such that each node (vertex) of the graph is represented by a CM cluster and every edge by the CF bridge. The resulting steady-state sequence of the bio-oscillators represents a unique ordering of phases where the adjacent nodes belong to an independent set. This ordering can subsequently be partitioned into independent sets using a simple polynomial time operation that compares the sequence to the adjacency matrix of the graph to identify the partition between two independent sets. Using standard graph theory, the nodes of a partition (independent set) can be assigned a unique color. For the representative graph considered in Figure 4, it can be observed that the bio-oscillators settle to a steady state where the bio-oscillator phases have the following cyclic ordering: ...1, 9, 2, 6, 4, 8, 5, 3, 7.... Subsequently, this ordering can be partitioned into three distinct independent sets {2,9}{6,4,8}{5,3,7,1}. Assigning each such set a color implies that a minimum of three colors are required to “color” the graph. Furthermore, we also explore using circuit simulation, the potential of the system to be scaled to a larger number of nodes. In such cases, the intrinsic parallelism of coupled oscillator networks is expected to yield a significant performance advantage over traditional heuristic-based Boolean computer hardware. Using the oscillator and the fibroblast equivalent model (described in detail in the Supporting Information) simulated in Xyce,^[23] we analyze the ability of the system to color representative graph instances from the DIMACS data challenge. As described earlier, the steady-state phase sequence of the oscillators is used to construct the coloring solution. It can be observed that in larger graphs the solutions become suboptimal. We therefore propose a simple polynomial postprocessing scheme (described in the Supporting Information) to augment the solution (Figure S5, Supporting Information). For many NP-hard graph problems (including graph coloring), the solution to one problem can be decomposed into the solution of another hard problem (using polynomial time postprocessing). We therefore believe that the hardware substrate demonstrated here will be able to address a broader spectrum of graph problems.

In summary, we demonstrated the feasibility of coupled oscillator networks made of living CM cells, or bio-oscillators, as a physical biocomputational substrate for solving constrained optimization problems like vertex coloring of graphs. While current

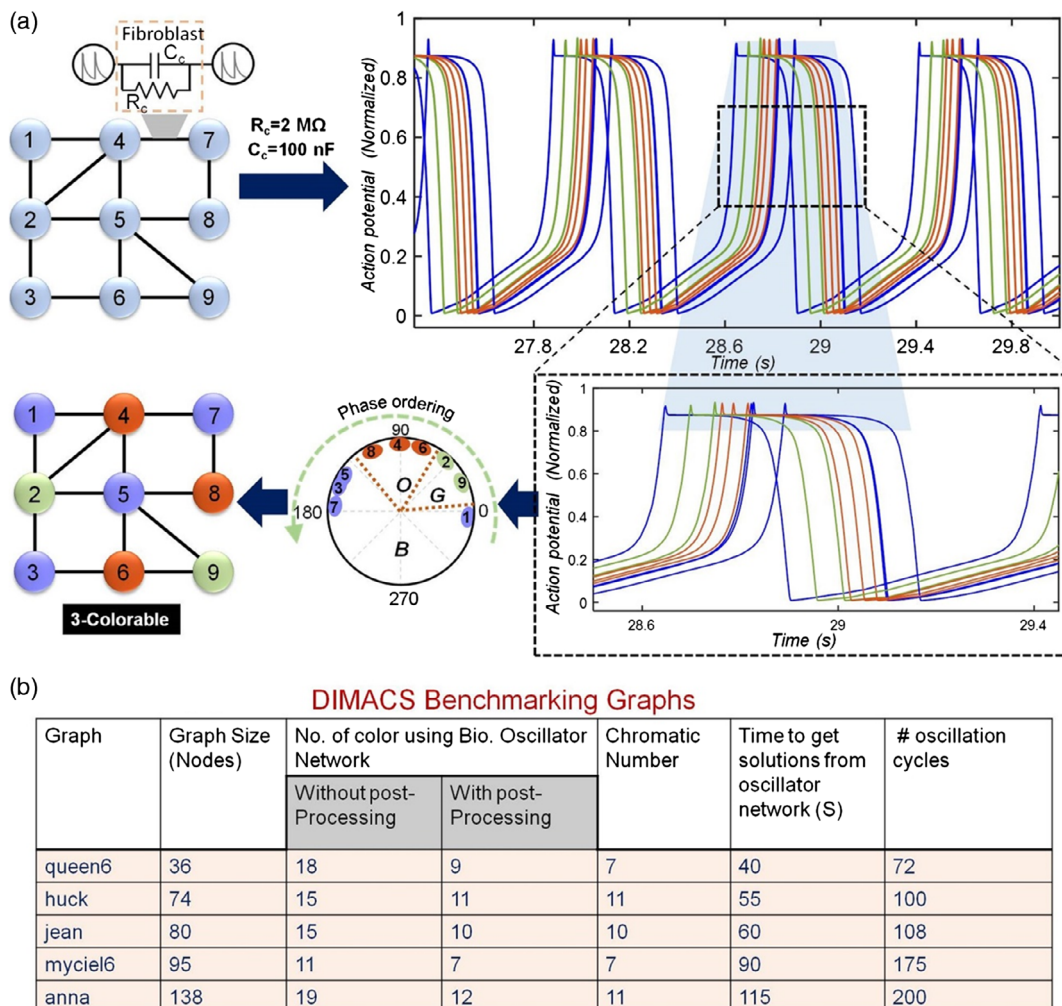


Figure 4. Application of cardiac cell oscillators to solve the minimum vertex coloring problem. a) Following the arrow flow: representative graph; time domain waveforms of its topologically equivalent coupled cardiac cell oscillator circuit; inset shows a single time period for each oscillator polar phase plot showing the relative phase difference among the oscillators; Resulting coloring solution obtained from the phase dynamics of the oscillators. b) Coloring solutions computed by the oscillators for graphs from the DIMACS implementation challenge.

approaches in biocomputation have so far been successful in archival data storage, they still fail to compete with silicon-based digital electronics in terms of parallel data processing. Data processing through genetic manipulations requires timescales that are much longer than those that are required for majority of computational tasks and input/output strategies are not compatible with conventional silicon-based technologies. Furthermore, in such systems, processing and communication are mostly implemented by altering molecules which are irreversible and not programmable/reconfigurable once built.^[24] Therefore, there is a big gap between current biocomputing approaches and future high-speed, large-scale data processing and transmission requirements. Currently, there is no cell-based biocomputing circuitry that operates as cell-scale networks and process information carried by electrical signals. The results of this research usher in a new paradigm to the emerging field of biocomputing; in contrast to the conventional approach of creating biocircuits using genetic manipulation of the cell as well as introducing chemicals and biomolecules, this study shows that cell-scale

networks and their natural ability to communicate with each other and synchronize to a state with unique phase pattern can be used as a computational primitive for efficiently solving computationally hard problems.

Supporting Information

Supporting Information is available from the Wiley Online Library or from the author.

Acknowledgements

The authors would like to thank Bradley Ellis, George Ronan, and Nicolas Chong for participating in rat cell isolation. The wafer molds were fabricated in the Notre Dame Nanofabrication Facility (NDNF). National Science Foundation (NSF) Electrical, Communication & Cyber Systems (ECCS) under award number 1807551; Semiconductor Research Corporation (SRC) under award number 2841.001.

Conflict of Interest

The authors declare no conflict of interest.

Author Contributions

P.Z., S.D., N.S., and H.C.C. initiated the ideas and research goals; X.R. and J.J. conducted experiments and data collection; I.C. participated in rat cell isolation and preliminary experiments on MEA; J.G. and M.K.B. performed data analysis; M.K.B., N.S., and S.D. did simulations; all authors discussed the results and discovered the scientific findings; P.Z., S.D., N.S., X.R., and J.G. wrote the original text and SI; S.D. and H.C.C. edited the manuscript; P.Z. and S.D. provided guidance over the research work.

Keywords

biocomputing, bio-oscillator, cardiomyocytes, collective computing

Received: November 10, 2020

Revised: December 8, 2020

Published online:

- [1] A. Parihar, N. Shukla, M. Jerry, S. Datta, A. Raychowdhury, *Sci. Rep.* **2017**, *7*, 1.
- [2] Y. Benenson, *Nat. Rev. Genet.* **2012**, *13*, 455.
- [3] R. Daniel, J. R. Rubens, R. Sarapeshkar, T. K. Lu, *Nature* **2013**, *497*, 619.
- [4] a) A. A. Green, P. A. Silver, J. J. Collins, P. Yin, *Cell* **2014**, *159*, 925; b) S. S. Damle, E. H. Davidson, *Proc. Natl. Acad. Sci.* **2012**, *109*, 1548; c) S. Regot, J. Macia, N. Conde, K. Furukawa, J. Kjellén, T. Peeters, S. Hohmann, E. De Nadal, F. Posas, R. Solé, *Nature* **2011**, *469*, 207; d) S. Ausländer, D. Ausländer, M. Müller, M. Wieland, M. Fussenegger, *Nature* **2012**, *487*, 123; e) J. Hasty, D. McMillen, J. J. Collins, *Nature* **2002**, *420*, 224; f) B. H. Weinberg, N. H. Pham, L. D. Caraballo, T. Lozanowski, A. Engel, S. Bhatia, W. W. Wong, *Nat. Biotechnol.* **2017**, *35*, 453.
- [5] J. Li, A. A. Green, H. Yan, C. Fan, *Nat. Chem.* **2017**, *9*, 1056.
- [6] J. Elbaz, O. Lioubashevski, F. Wang, F. Remacle, R. D. Levine, I. Willner, *Nat. Nanotechnol.* **2010**, *5*, 417.
- [7] a) D. Ausländer, S. Ausländer, X. Pierrat, L. Hellmann, L. Rachid, M. Fussenegger, *Nat. Methods* **2018**, *15*, 57; b) M. Müller, S. Ausländer, A. Spinnler, D. Ausländer, J. Sikorski, M. Folcher, M. Fussenegger, *Nat. Chem. Biol.* **2017**, *13*, 309.
- [8] U. I. Can, N. Nagarajan, D. C. Vural, P. Zorlutuna, *Adv. Biosyst.* **2017**, *1*, 1600035.
- [9] a) A. Goni-Moreno, P. I. Nikel, *Front. Bioeng. Biotechnol.* **2019**, *7*, 40; b) L. Grozinger, M. Amos, T. E. Gorochowski, P. Carbonell, D. A. Oyarzún, R. Stoof, H. Fellermann, P. Zuliani, H. Tas, A. Goñi-Moreno, *Nat. Commun.* **2019**, *10*, 1.
- [10] a) L. Personnaz, I. Guyon, G. Dreyfus, *Phys. Rev. A* **1986**, *34*, 4217; b) S. T. Keene, C. Lubrano, S. Kazemzadeh, A. Melianas, Y. Tuchman, G. Polino, P. Scognamiglio, L. Cinà, A. Salleo, Y. van de Burgt, *Nat. Mater.* **2020**, *19*, 969; c) A. Gidon, T. A. Zolnik, P. Fidzinski, F. Bolduan, A. Papoutsi, P. Poirazi, M. Holtkamp, I. Vida, M. E. Larkum, *Science* **2020**, *367*, 83.
- [11] a) G. Beni, J. Wang, in *Robots and Biological Systems: Towards a New Bionics?*, Springer, Berlin/New York **1993**, p. 703; b) J. Baumgardner, K. Acker, O. Adefuye, S. T. Crowley, W. DeLoache, J. O. Dickson, L. Heard, A. T. Martens, N. Morton, M. Ritter, *J. Biol. Eng.* **2009**, *3*, 11.
- [12] J. Stricker, S. Cookson, M. R. Bennett, W. H. Mather, L. S. Tsimring, J. Hasty, *Nature* **2008**, *456*, 516.
- [13] L. Zhu, S.-J. Kim, M. Hara, M. Aono, *R. Soc. Open Sci.* **2018**, *5*, 180396.
- [14] a) N. Agladze, O. Halaidych, V. Tsvelaya, T. Bruegmann, C. Kilgus, P. Sasse, K. Agladze, *Biomater. Sci.* **2017**, *5*, 1777; b) T. Kaneko, K. Kojima, K. Yasuda, *Biochem. Biophys. Res. Commun.* **2007**, *356*, 494.
- [15] S. Dutta, A. Parihar, A. Khanna, J. Gomez, W. Chakraborty, M. Jerry, B. Grisafe, A. Raychowdhury, S. Datta, *Nat. Commun.* **2019**, *10*, 1.
- [16] A. Parihar, N. Shukla, S. Datta, A. Raychowdhury, *J. Appl. Phys.* **2015**, *117*, 054902.
- [17] A. Mallick, M. K. Bashar, D. S. Truesdell, B. H. Calhoun, S. Joshi, N. Shukla, *Nat. Commun.* **2020**, *11*, 1.
- [18] J. Fu, J. Gao, R. Pi, P. Liu, *Cytotechnology* **2005**, *49*, 109.
- [19] R. Plonsey, R. C. Barr, *Bioelectricity: A Quantitative Approach*, Springer Science & Business Media, New York, NY **2007**.
- [20] M. S. Spach, R. C. Barr, G. A. Serwer, J. M. Kootsey, E. A. Johnson, *Circ. Res.* **1972**, *30*, 505.
- [21] G. Gaudesius, M. Miragoli, S. P. Thomas, S. Rohr, *Circ. Res.* **2003**, *93*, 421.
- [22] a) Y. Maeda, E. Yagi, H. Makino, *BioSystems* **2005**, *79*, 125; b) G. Massobrio, L. Massobrio, *J. Comput. Electron.* **2013**, *12*, 43.
- [23] E. R. Keiter, T. Mei, T. V. Russo, R. L. Schiek, P. E. Sholander, H. K. Thornquist, J. C. Verley, D. G. Baur, *XyceTM Parallel Electronic Simulator Reference Guide, Version 6.3*, Sandia National Lab.(SNL-NM), Albuquerque, NM; Raytheon Albuquerque, NM **2015**.
- [24] Y. Benenson, *Nat. Nanotechnol.* **2011**, *6*, 465.